UNIVERSITY OF ZIELONA GÓRA

CEER CIVIL AND ENVIRONMENTAL ENGINEERING REPORTS

CIVIL AND ENVIRONMENTAL ENGINEERING REPORTS

E-ISSN 2450-8594

CEER 2026; 36 (3): 0102-0117
DOI: 10.59440/ceer/235853
Original Research Article

URBAN WATER BUDGET ASSESSMENT BASED ON ALS AND SATELLITE HYDROLOGICAL DATA

Monika BIRYŁO[1], Michał BEDNARCZYK[1], Wioleta BŁASZCZAK-BĄK[1], Anna SOBIERAJ-ŻŁOBIŃSKA[2]
[1]Faculty of Geoengineering, University of Warmia and Mazury in Olsztyn, Olsztyn, Poland
[2]Faculty of Civil and Environmental Engineering, Gdańsk University of Technology, Gdańsk, Poland

Abstract

Urbanization modifies hydrological processes by altering water balance components and increasing drought vulnerability. This study proposes an integrated multi-scale framework combining airborne laser scanning (ALS)-based terrain classification with satellite-derived hydrological datasets (GLDAS and GRACE/GRACE-FO) to assess urban water budget (WB) dynamics. ALS data were used to identify permeable and impervious surfaces, while time-series decomposition was applied to evaluate trends, seasonality, and variability of WB components.

The results show that permeable surfaces dominate the study area (71.23%), limiting surface runoff. The WB demonstrates pronounced seasonal variability, with increased fluctuations after 2015, while long-term trends remain statistically insignificant. Surface sealing corrections for evapotranspiration and runoff strongly correspond with the original WB (R = 0.977 and R = 0.998), confirming precipitation as the main controlling factor. The proposed framework improves the representation of urban hydrological processes by linking detailed surface characteristics with large-scale climate observations and supports urban water management and climate adaptation planning.

Keywords: urban hydrology, water budget, ALS, GRACE, evapotranspiration

1. INTRODUCTION

Rapid climate change and ongoing urbanization are increasingly affecting hydrological processes, creating a need for improved understanding of water-cycle dynamics in urban environments. Urban expansion modifies land-surface characteristics and alters water balance components, influencing drought development, water availability, and hydrological variability. Although precipitation patterns

[2] Corresponding author: Faculty of Civil and Environmental Engineering, Gdańsk University of Technology, Narutowicza 11/12, 80-233 Gdańsk, Poland, anna.sobieraj-zlobinska@pg.edu.pl
[1]Faculty of Geoengineering, University of Warmia and Mazury in Olsztyn, Oczapowskiego 2, 10-719 Olsztyn, Poland, monika.sienkiewicz@uwm.edu.pl

are primarily controlled by large-scale atmospheric processes, urbanization can substantially modify evapotranspiration, infiltration, and surface runoff. The replacement of vegetated areas by impervious surfaces reduces infiltration capacity and groundwater recharge while increasing rapid runoff generation and peak flow response. As a result, urban areas may experience enhanced hydrological variability, characterized by short periods of intensive runoff followed by prolonged water deficits caused by limited subsurface recharge [Wałęga et al., 2019; Pasquier et al., 2022; Mazrooei et al., 2021; Liu et al., 2021].

Accurate identification of terrain characteristics and land-cover structure is therefore essential for understanding spatial variability in urban hydrological processes. The distribution and arrangement of permeable and impervious surfaces directly influence infiltration, runoff generation, and local water retention. High-resolution datasets derived from Airborne Laser Scanning (ALS) provide detailed information on terrain morphology and surface structure, enabling improved assessment of fine-scale hydrological variability. However, local-scale datasets alone do not capture regional hydrological dynamics and long-term changes in water storage.

In contrast, global hydrological products provide consistent observations of water-cycle components over large spatial and temporal scales. The Global Land Data Assimilation System (GLDAS) enables estimation of precipitation (P), evapotranspiration (EV), and surface runoff (SRO), while satellite gravimetry missions such as the Gravity Recovery and Climate Experiment (GRACE) and GRACE Follow-On (GRACE-FO) provide observations of total water storage (TWS) anomalies. Despite their importance for regional and global hydrological assessments, these datasets do not represent local surface heterogeneity, which strongly controls infiltration and runoff processes in urbanized areas.

Previous studies have focused mainly on either large-scale climatic controls or local impacts of land-use change [Salazar et al., 2024; Seager et al., 2014; Zhu et al., 2024; Yilmaz et al., 2019; Claessens et al., 2006]. However, limited research has integrated high-resolution urban surface characterization with satellite-based hydrological observations and water balance indicators [Guizaini et al., 2024; Dujardin et al., 2011]. This methodological gap restricts the understanding of how urban surface structure influences water balance variability under changing climatic conditions.

Therefore, this study develops and applies an integrated multi-scale framework combining ALS-derived terrain classification with satellite-based hydrological observations (GLDAS and GRACE/GRACE-FO) to assess urban water balance dynamics and their temporal variability. The proposed approach links fine-scale surface permeability information with long-term hydrological time-series analysis to quantify urban water balance components, evaluate drought-related variability, identify trends and seasonal patterns, and determine the influence of terrain structure on local hydrological responses. The framework provides a transferable approach for improved urban hydrological assessment and supports sustainable water management and climate adaptation strategies.

Unlike previous studies that analyse either local surface characteristics or regional hydrological observations separately, the proposed framework explicitly combines both spatial scales. This enables the simultaneous consideration of detailed urban surface properties and long-term climatic variability, providing a more comprehensive assessment of urban water budget dynamics. This integration also directly provides a scalable tool for environmental engineers to design sustainable urban drainage systems and optimize hydraulic infrastructure under climate pressures.

2. DATA SOURCES AND COLLECTION

The study area covers the Kortowo academic campus and part of adjacent districts, located in the south-western part of Olsztyn, Warmian-Masurian Voivodeship, north-eastern Poland. The area belongs to the University of Warmia and Mazury and serves educational, residential, administrative, and recreational functions (Fig. 1).

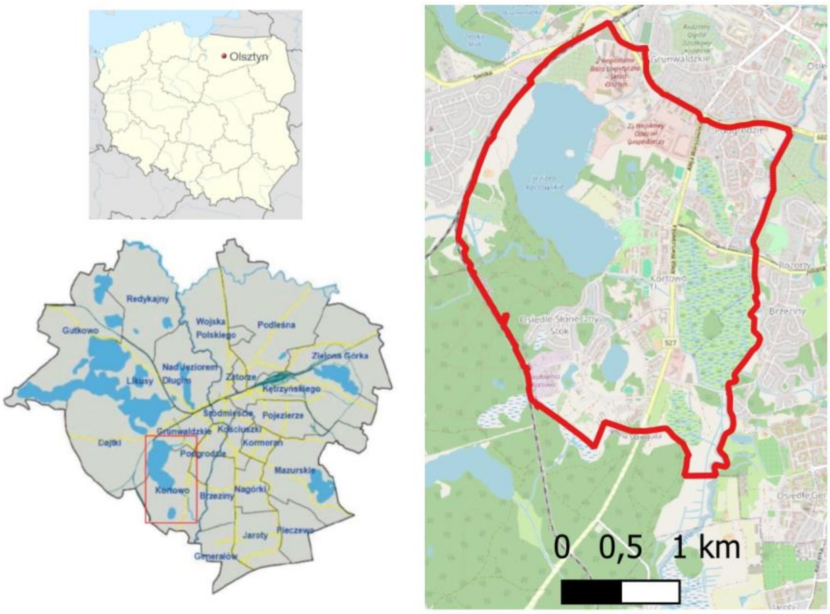

Fig. 1. Location of the Olsztyn and Kortowo academic campus

Land use within the study area is diverse, including buildings, transportation infrastructure, parking areas, and extensive green spaces. Surface water bodies, including Kortowskie Lake, play an important role in shaping local hydrological conditions. The area exhibits a mosaic of permeable and impervious surfaces. Impervious surfaces mainly consist of roofs, roads, and paved areas, while permeable surfaces include green areas and unsealed soils. Moderately varied post-glacial topography affects stormwater runoff directions and local retention.

2.1. ALS data

The analyses were conducted using ALS data obtained from the National Geoportal, comprising 36 tiles. The point cloud was clipped to the study area's spatial extent. The point cloud density was 12 points/m², enabling detailed analysis of surface structure. The mean vertical and horizontal positional errors were 0.10 m and 0.25 m, respectively. The data were acquired in 2023 and processed in the PL-1992 horizontal coordinate reference system and the PL-EVRF2007-NH vertical reference system. The spatial extent of the research area and ALS tile coverage is shown in Figure 2.

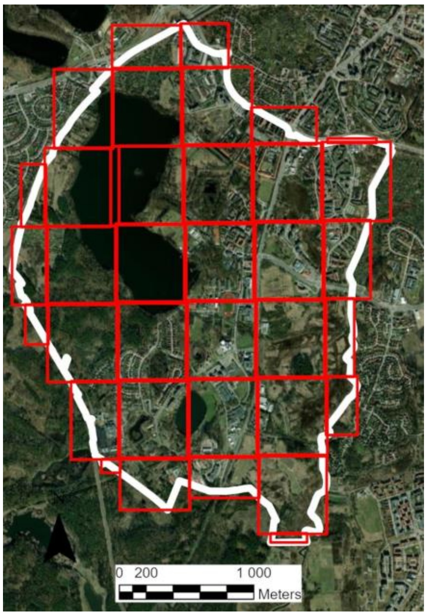

Fig. 2. Location of the Kortowo and adjacent districts (study area; white outline) with ALS tile coverage (red squares).

2.2. Hydrological data

The following types of observations were used in the research: total water storage, precipitation, evapotranspiration, and surface runoff.

Precipitation (P) is an essential part of the hydrological cycle, bringing water from the atmosphere to the Earth's surface. Evapotranspiration (EV) is the sum of all processes that result in the movement of water from the Earth's surface to the atmosphere through evaporation from soil and water bodies and transpiration from vegetation. Rainwater that does not infiltrate the soil is subject to surface runoff (SRO). All these observations can be downloaded from GLDAS, an extremely important data source for studies of the global water cycle. GLDAS is a global land surface modelling system [Rodell et al. 2004]. It supports four sub-models: Noah, the Community Land Model (CLM), the Variable Infiltration Capacity (VIC), and Mosaic. GLDAS provides spatially resolved environmental change studies at grid resolutions of 1°×1° and 0.25°×0.25° [Wang et al., 2016].

Total water storage (TWS) is a holistic measure that includes surface water, groundwater, snow and atmospheric water [Sun et al., 2024]. TWS observations, calculated from gravity models, can be obtained thanks to the GRACE and GRACE-FO satellite missions. The mission's goal is to provide monthly models of the time-varying gravity field [Hacker and Kusche, 2024; Tapley et al., 2019]. A major achievement of the mission is to investigate the natural variability of the hydrological cycle on land by determining groundwater stress [Rzepecka et al., 2024; Richey et al., 2015], drought [Zhao et al., 2017], and soil processes [Swenson and Lawrence, 2014].

The water budget (WB) components were examined in the study area (Fig. 2). Precipitation amplitude ranges between $1.0 \cdot 10^{-5}$ and $7.0 \cdot 10^{-5}$ kg/m²/s. A distinct seasonality is observed, with the highest values in the summer months and the lowest in spring and autumn (Fig. 3). Outliers are noticeable (e.g., $6.9 \cdot 10^{-5}$ kg/m²/s in August 2006 or $6.8 \cdot 10^{-5}$ in July 2011). It was also noted that many years after 2012 had significantly higher peaks than previous years. The most consistent signal of the three studied years was observed for evapotranspiration. High values are noticeable from May to September, dropping to near 0 in winter. The lowest values were found for surface runoff (ranging from $0.1 \cdot 10^{-5}$ kg/m²/s to $0.5 \cdot 10^{-5}$ kg/m²/s). The highest values usually appear after the maximum P values. Low SRO values indicate that the studied area is characterized by high infiltration. These hydrological datasets constitute the temporal component of the analysis, complementing the spatial information derived from ALS classification. Their integration enables assessment of how terrain structure influences variability in WB components.

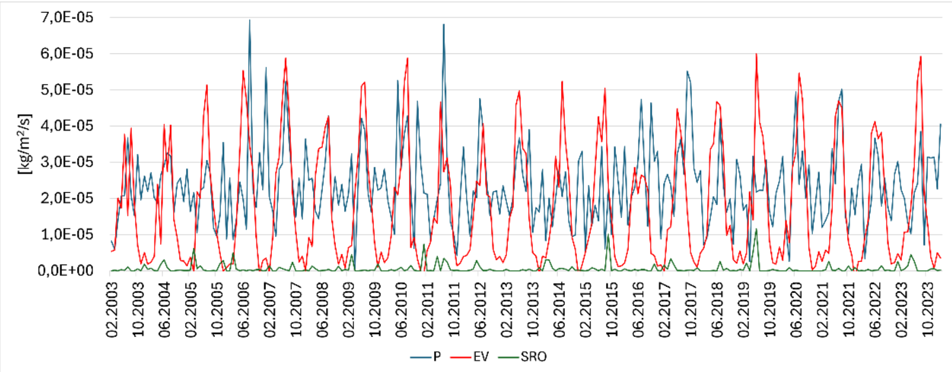

Fig. 3. WB components: precipitation (P), evapotranspiration (EV), and surface runoff (SRO)

3. METHODOLOGY

The methodology adopted in this study follows a sequential analytical framework that integrates high-resolution terrain data with hydrological time-series analysis. The workflow consists of seven main stages.

Stage 1: Land Cover Classification and Permeability Assessment

The first stage aimed to derive a spatially explicit representation of permeable and impervious surfaces from high-resolution ALS data, as shown in Figure 4.

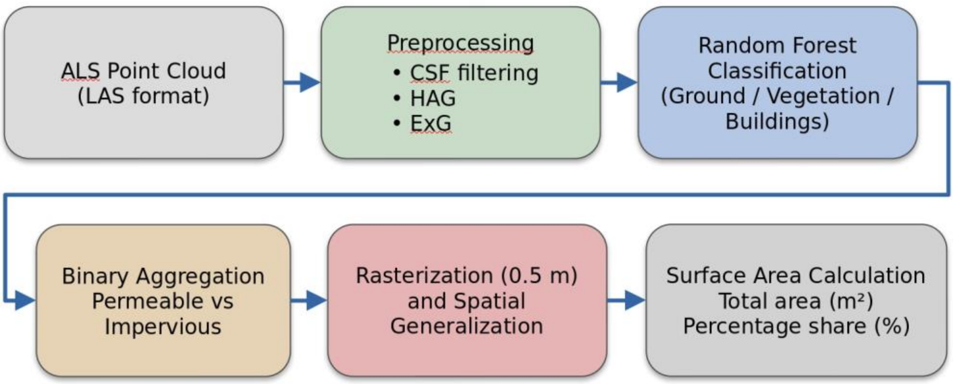

Fig. 4. ALS surface permeability workflow diagram

All processing was implemented in Python to ensure reproducibility and scalability. The workflow was designed for automated batch processing of multiple ALS tiles and subsequent aggregation into a unified raster layer. The following libraries were employed:

- PDAL – point cloud preprocessing, including ground filtering and height normalization,
- NumPy and Pandas – numerical computation and structured data handling,
- scikit-learn – implementation of the Random Forest classification algorithm,
- laspy – manipulation and export of LAS files with derived attributes,
- rasterio – rasterization and GeoTIFF generation.

The entire procedure was executed at the native resolution of the ALS dataset prior to raster aggregation. The ALS point cloud (LAS format) was processed to extract terrain structure and surface characteristics relevant to permeability assessment.

To preserve traceability and avoid loss of reliable pre-classified features, the original ALS classification was retained in a separate attribute before further processing. Ground points were separated using the Cloth Simulation Filter (CSF), which simulates a cloth surface draped over the point cloud to distinguish terrain from above-ground objects. Subsequently, the Height Above Ground (HAG) parameter was computed for each point using nearest-neighbour interpolation. To enhance vegetation detection, the Excess Green Index (ExG) was derived from normalized RGB values:

$$ExG = 2g - r - b \tag{3.1}$$

where *r*,*g*,*b* represent the normalized red, green, and blue channels, respectively.

For supervised classification, a Random Forest classifier was used to distinguish between three primary surface categories: ground, vegetation, and buildings. The classification was based on a feature set comprising:

- Height Above Ground,
- Excess Green Index,
- return intensity,
- number of returns.

The machine learning output was integrated with the preserved original ALS point cloud classification to ensure consistency in building detection and minimize misclassification of vertical structures. The next step of processing was aggregation into permeability classes. Following multi-class classification, the dataset was reduced to two functional surface categories:

- permeable surfaces, including vegetation and natural (unsealed) ground,
- impervious surfaces, including buildings and sealed ground surfaces such as asphalt and concrete.

Rule-based criteria incorporating spectral and height thresholds were used to distinguish sealed ground from natural soil.

The conversion from the classified ALS point cloud to the final permeability map was based on the hydrological function of each surface class rather than on its geometric characteristics. Vegetation and natural ground classes were assigned to the permeable category because they allow infiltration and evapotranspiration, whereas buildings, together with sealed transport surfaces (roads, pavements and parking areas), were classified as impervious due to their limited infiltration capacity. This aggregation simplified the original multi-class classification into two hydrologically meaningful classes used in the subsequent water budget calculations.

The next step was rasterization and spatial generalization. The classified point cloud was rasterized at a spatial resolution of 0.5 m.

For each raster cell, class assignment was determined using a majority-based rule. To ensure stable representation of buildings, a threshold condition was applied: if at least 40% of the points within a cell were classified as buildings, the cell was assigned to the impervious class. This constraint reduces edge effects and minimizes fragmentation of vertical structures.

Areas without laser scanning returns (e.g., water bodies or acquisition gaps) were marked as no-data and excluded from area calculations to prevent artificial bias in permeability estimates.
Surface areas (A) were computed as:

$$A = N * p^2 \tag{3.2}$$

where: N is the number of raster cells assigned to a given class, p is the raster resolution.

The final outputs include the absolute surface area (m²) and the percentage shares of permeable and impervious surfaces within the analyzed domain.

Stage 2: Baseline Water Budget Calculation

The WB is the difference between the recharge and discharge of water into a system. In this study, the term water budget refers to a simplified hydrological balance calculated using the hydrological variables available from the GLDAS dataset, namely P, EV, and SRO. Consequently, the proposed formulation does not represent the complete water balance, as processes such as groundwater exchange, infiltration, anthropogenic water use, and changes in soil moisture storage are not explicitly included. The adopted formulation is intended to quantify the dominant climatic controls on urban hydrological variability while enabling consistent long-term comparisons. The baseline WB was calculated using unmodified hydrological parameters obtained from GLDAS and GRACE/GRACE-FO according to formula [Birylo et al., 2018, Birylo et al., 2025]:

$$WB = P - EV - SRO \tag{3.3}$$

where: P, EV and SRO are hydrological parameters obtained from GLDAS.

Stage 3: Time-Series Decomposition of Water Budget

To investigate temporal variability, the WB time series was decomposed into trend, seasonal, and random components using an additive model:

$$TimeSeries = Trend + Seasonal + Noise \tag{3.4}$$

After smoothing the original series using a moving average, the trend component was extracted and removed:

$$DetrendedTimeSeries = TimeSeries - Trend \tag{3.5}$$

The seasonal component was determined by averaging values for the corresponding periods across years, while the remaining variability constituted the random noise component. This decomposition allowed identification of long-term tendencies, cyclical patterns, and stochastic anomalies in the water budget.

Stage 4: Modification of Evapotranspiration Accounting for Surface Sealing

Urbanization significantly affects evapotranspiration by reducing the area covered by vegetation. To account for this effect, a modified evapotranspiration value was introduced, based on the sealed-surface share derived from ALS classification. Based on the simplified form of the Penman–Monteith equation [Penman, 1948; Monteith et al., 1965] proposed by Błaszczak-Bąk et al. [2025], evapotranspiration was calculated as follows:

$$EV_{modified} = (1 - f_{sealed})EV \tag{3.6}$$

where $EV_{modified}$ is the evaporation value after introducing the influence of impermeable surfaces, f_{sealed} is the share of sealed surface, $(1 - f_{sealed})$ and is the share of surface area that allows evapotranspiration.

Stage 5: Modification of Surface Runoff Accounting for Impervious Areas

Impervious surfaces directly increase surface runoff by reducing infiltration capacity. To quantify this effect, surface runoff was modified following the approach of Brabec et al. [2002]:

$$SRO_{modified} = SRO \cdot (1 + \alpha f_{sealed}) \tag{3.7}$$

where α is the relative influence of f_{sealed} on surface runoff.

To determine the parameter α optimally, the ratio of surface runoff to precipitation was calculated to quantify the proportion of precipitation converted into rapid runoff. This ratio represents the percentage change in surface runoff (SRO) associated with a one-unit increase in the fraction of sealed surfaces (f_{sealed}):

$$R = \frac{SRO}{P} \tag{3.8}$$

To establish the relationship between R and f_{sealed} linear regression was performed:

$$R \sim f_{sealed} \tag{3.9}$$

Climatic control was incorporated using the Composite Climate–Drought Index (CCDI):

$$R = f_{sealed} + CCDI \tag{3.10}$$

The CCDI index was calculated as:

$$CCDI = \frac{CD - \underline{CD}}{st.dev.(CD)} \tag{3.11}$$

Where CD (Climate Drought):

$$CD = PA^R + TWSA^R \tag{3.12}$$

with PA^R and $TWSA^R$ representing precipitation anomaly and terrestrial water storage anomaly residues, respectively.

The interaction between surface sealing and climatic conditions was tested for statistical significance using the model:

$$R = f_{sealed} + CCDI + f_{sealed} * CCDI \tag{3.13}$$

The integration bridges spatial scales by utilizing the high-resolution ALS structural ratios as direct downscaling variables to recalibrate regional GLDAS observations down to the urban canopy level, as formalized in equations (3.6) and (3.7).

Stage 6: Comparison of Water Budget Variants

Following the modifications, three WB variants were available for comparative analysis:

- WB – calculated using original GLDAS-derived EV and SRO
- WB_EV$_{modified}$ – calculated with modified evapotranspiration (EV$_{modified}$)
- WB_SRO$_{modified}$ – calculated with modified surface runoff (SRO$_{modified}$)

Correlation coefficients between time series were computed to assess temporal pattern similarity and to identify the relative contribution of each modification to overall WB variability.

Stage 7: Trend and Seasonality Analysis

The final analytical stage focused on a detailed examination of temporal patterns in all WB variants. The extracted trend component was analyzed to detect any systematic long-term changes in water availability. The seasonal component was examined for regularity and stability of amplitude across the study period. The random noise component was assessed for patterns that might indicate anomalous hydrological events not captured by regular seasonal cycles.

Additionally, the CCDI series underwent the same decomposition procedure to compare patterns of climatic variability with WB dynamics. This comprehensive temporal analysis enabled the identification of the dominant factors controlling variability in the water budget of the urbanized study area.

The adopted methodology has several limitations to consider when interpreting the results. Surface classification accuracy depends on local ALS point density, which can increase uncertainty in sparsely sampled areas, particularly along object edges. The ExG, based solely on RGB information, is sensitive to illumination conditions, material reflectance variability, and seasonal effects. Open water surfaces were not directly classified due to the absence of laser scanning returns and were treated as no-data areas. Additionally, the rule-based generalization using a 40% building threshold may slightly overgeneralize building boundaries. Despite these limitations, the workflow provides spatially consistent and reproducible estimates of surface permeability suitable for further modelling applications.

4. RESULTS

The application of the integrated methodology described in the previous section yielded a series of results corresponding to each analytical stage. This section presents the outcomes of land cover classification, baseline WB calculations, time-series decomposition, and the effects of modifications to evapotranspiration and surface runoff. The results are organized sequentially to demonstrate how terrain structure information progressively refines the assessment of urban water balance dynamics.

In **Stage 1**, land cover classification was performed, and the distributions of permeable and impervious surfaces were derived. Based on the classified point cloud, additional thematic classes were extracted, including roads, sidewalks, pedestrian and bicycle paths, parking areas and paved squares, derived from the original ground class. Subsequently, the point cloud was aggregated into two functional classes representing permeable and impervious surfaces, which served as the basis for further hydrological analyses.

The spatial distribution of classified surfaces is shown in Figure 5, where permeable and impervious structures derived from ALS data serve as the basis for subsequent calculations.

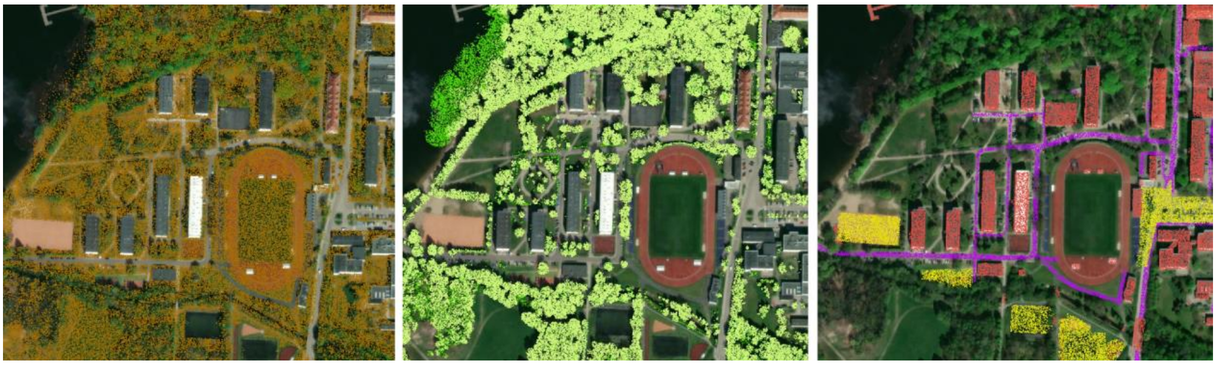

Fig. 5. Examples of permeable and impervious surfaces - point cloud classes: ground - permeable (left); vegetation low–high - permeable (middle); buildings, roads, pavements, bicycle path, asphalt square/parking lot - impervious (right); orthophotomap is used as basemap

Based on the extracted classes, two datasets representing permeable and impervious areas were prepared. They are presented in Figure 6.

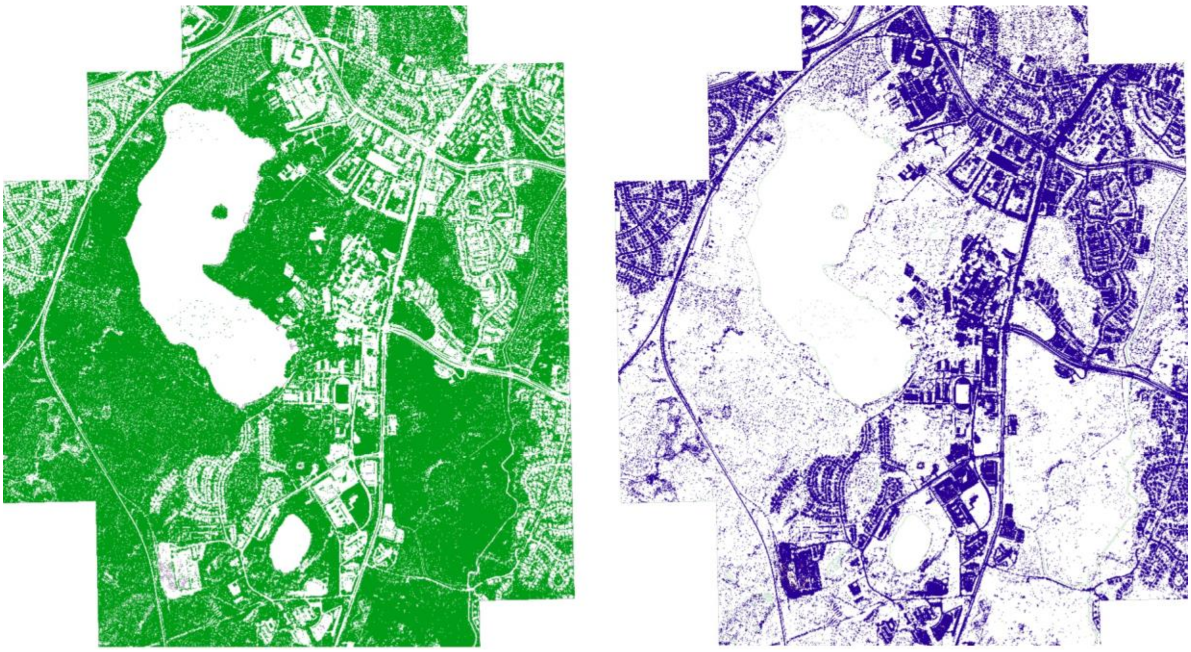

Fig. 6. Point classes represented: permeable surface (left) and impervious surface (right)

Given the adopted land-cover classification, the surface area share (A%) was calculated for each class. The results are summarized in Table 1. Additionally, the percentage of the area occupied by vegetation was distinguished separately because of its different influence on EV in the water budget calculations. The analyzed area covers 9,749,910 m² (excluding no-data areas), of which vegetation accounts for 67.47%. Permeable surfaces account for 71.23% of the area, while impervious surfaces account for 28.77%.

Table 1: Results of area share calculation

Total area (excluding no-data)	9 749 910 m²	100%
Vegetation	6 285 740 m²	67,47%
Permeable ground	6 944 983 m²	71,23%
Impervious ground	2 804 927 m²	28,77%

In **Stage 2**, the WB was computed from the model's precipitation, evapotranspiration, and surface runoff values using formula (3.3). Results are presented in Figure 7.

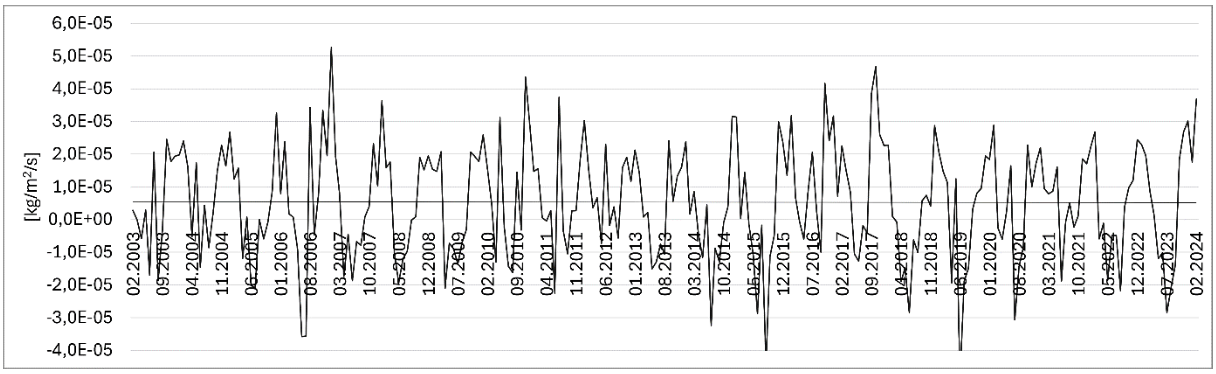

Fig. 7. WB computed for the Kortowo area

The computed WB time series shows substantial temporal variability. During the period 2003–2014, WB amplitudes remained relatively stable, ranging from $1.8\cdot10^{-5}$ to $2.4\cdot10^{-5}$ kg/m²/s, indicating conditions slightly above normal. An exception occurred at the turn of 2006 and 2007, when values ranged from $-3.5\cdot10^{-5}$ to $5.2\cdot10^{-5}$ kg/m²/s. Since 2015, continuous variability in amplitude has been observed. Except for 2016 and 2017, summer WB values were markedly low, reaching approximately $-5.0\cdot10^{-5}$ kg/m²/s, indicating below-normal conditions and limited replenishment of the water system. In 2016–2017, minimum values reached approximately $-1.0\cdot10^{-5}$ kg/m²/s, while maximum values approached $4.5\cdot10^{-5}$ kg/m²/s. The calculated linear trend equals $-4\cdot10^{-11}$ per year $R^2 = 3\cdot10^{-5}$, indicating the absence of a significant long-term tendency.

During **Stage 3,** the analyzed WB series were decomposed into trend, seasonality, and random noise components using the additive model. The results of this decomposition are presented in Figures 8-10.

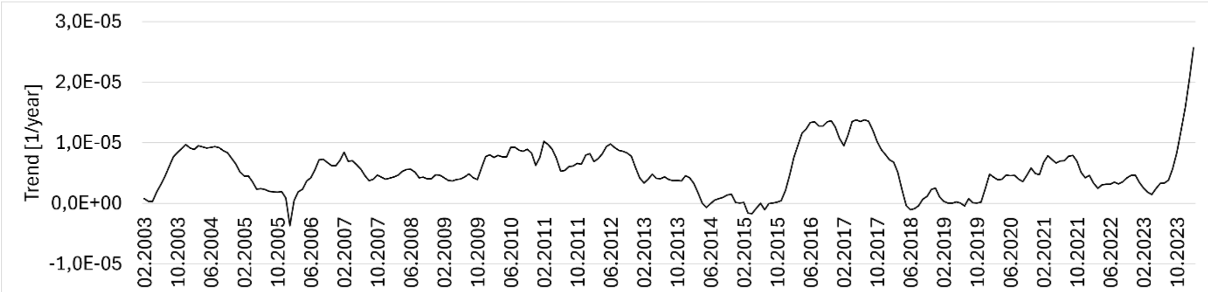

Fig. 8. Trend of the WB time series

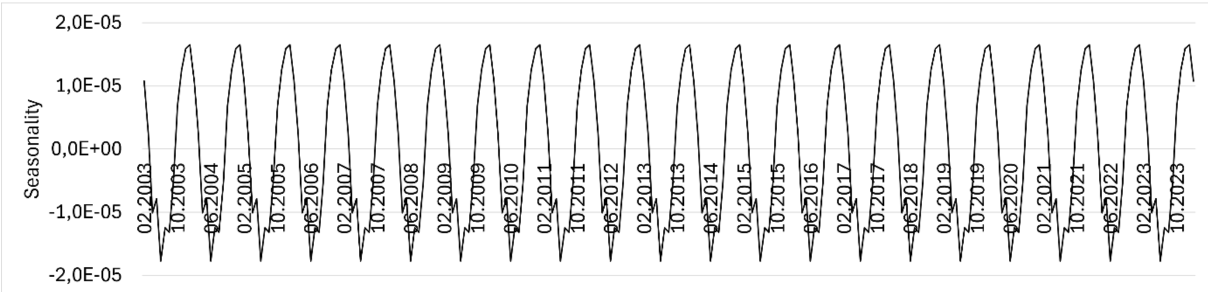

Fig. 9. Seasonality of the WB time series

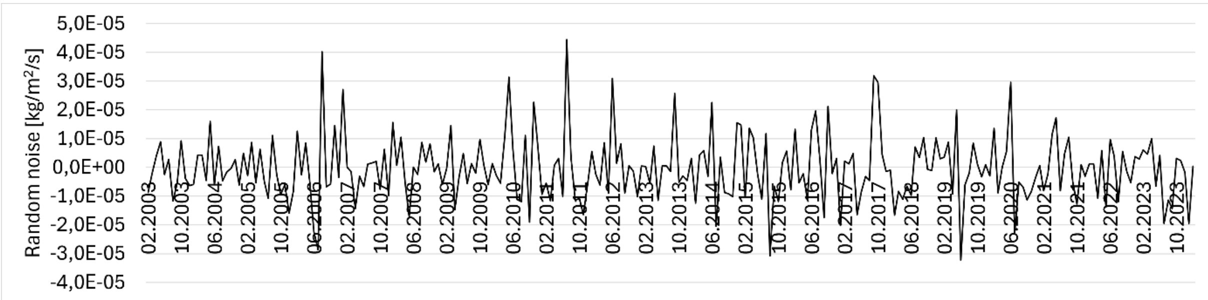

Fig. 10. Random noise of the WB time series

The extracted trend (Fig. 8) is relatively flat, with no significant short-term changes. Individual small local fluctuations (e.g., 2016–2017) are not systematic, indicating that long-term changes in the water budget are not dominated by monotonic trends. The smoothed curve represents the long-term trend, and its flatness suggests that budget changes are more closely related to seasonality and noise than to systematic directional change.

The seasonal component (Fig. 9) exhibits regular, cyclical, and repetitive patterns, varying from approximately $-1.7 \cdot 10^{-5}$ kg/m²/s in June to $1.5 \cdot 10^{-5}$ kg/m²/s in January. This regular annual cycle reflects the strong influence of seasonal climatic patterns on water availability in the study area.

The random noise component (Fig. 10) is highly variable and unstable, exhibiting no regular patterns. This irregularity reflects short-term hydrological anomalies and stochastic events rather than persistent cyclical or directional changes. The next **Stage 4** focused on modified WB. The same normal distribution was applied to the CCDI series. It was observed that the trend has a wave-like character, oscillating around 0. Seasonality exhibits very regular cycles with constant amplitudes ranging from -

1.11 (September) to 0.76 (March). Random Noise is characterized by random fluctuations around 0 and is not constant. The recalculated WB using modified evapotranspiration is presented in Figure 11.

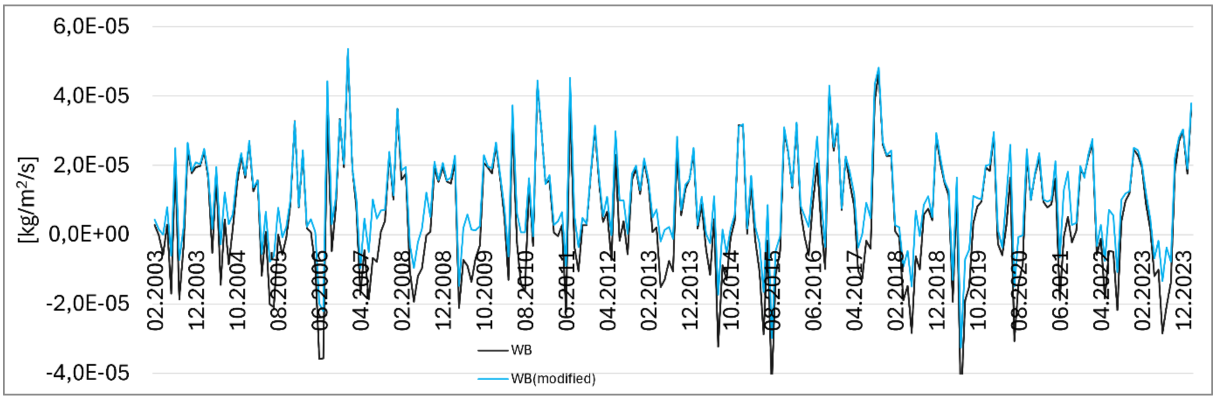

Fig. 11. Original and WB_EVmodified over time

A WB was calculated using a modified evapotranspiration approach. The correlation coefficient between the time series was 0.977. It was found that 1/4 of the study area is impermeable; therefore, precipitation is not absorbed into the ground, whereas evapotranspiration is significantly hindered. Modifying evapotranspiration allowed us to calculate the water budget using the modified evapotranspiration value. Analysis of the results revealed that the highest values remained unchanged, while the minimum values were lower, resulting in smaller amplitude changes.

Based on this analysis, the coefficient α was determined as 1.2 for the study area. The resulting modified water budget is shown in Figure 12.

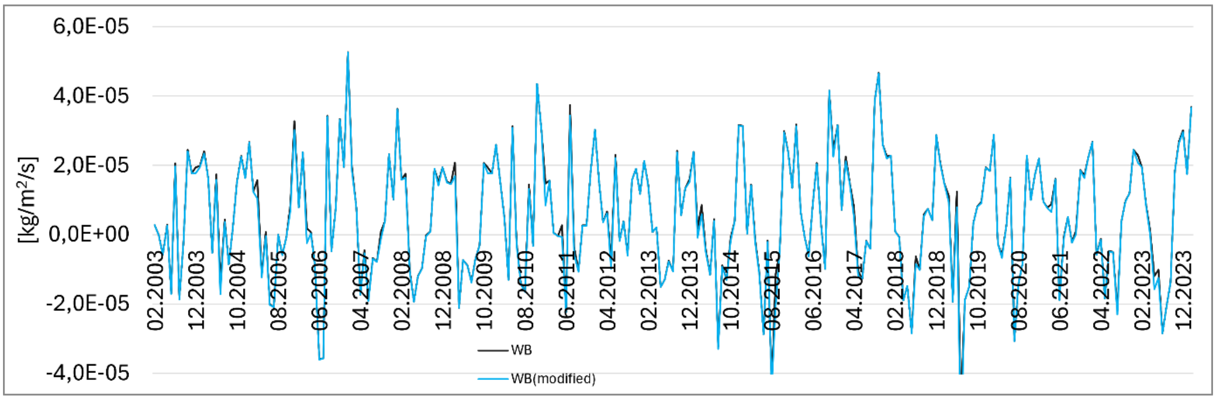

Fig. 12. Original and WB_SROmodified over time

The correlation coefficient between the water budget time series and the water budget with modified SRO was 0.998. Differences between the series occur mainly in individual peak values and do not significantly affect WB amplitudes, indicating that precipitation remains the dominant factor controlling variability in the water budget. Individual deviations from the raw WB course are evident in isolated maximum values, but they do not alter the WB amplitude.

Our research showed that precipitation is the primary factor influencing WB changes.

5. DISCUSSION

The results demonstrate that urban water balance dynamics are primarily controlled by seasonal climatic variability rather than long-term trends. This finding is consistent with previous studies indicating the dominant role of precipitation in short-term hydrological variability.

The high proportion of permeable surfaces (over 70%) explains the relatively low surface runoff observed in the study area. However, despite this favorable condition, increasing variability in WB amplitudes after 2015 suggests growing sensitivity to climatic fluctuations, potentially linked to ongoing climate change.

The integration of ALS-derived surface classification with global hydrological datasets represents a significant methodological advancement. Unlike traditional approaches that rely solely on large-scale models, the proposed framework incorporates spatial heterogeneity at high resolution, improving the interpretation of evapotranspiration and runoff processes.

Nevertheless, several limitations should be considered. The use of GLDAS data at coarse spatial resolution may not fully capture local variability, while the ExG index is sensitive to illumination and seasonal conditions. Future studies should incorporate higher-resolution meteorological data and explore additional spectral indices.

Future developments of the proposed methodology may include the incorporation of higher-resolution meteorological datasets, weather radar observations, Sentinel-based products, and additional remote sensing indicators describing vegetation condition and soil moisture. Such extensions could improve the representation of local hydrological processes and increase the applicability of the proposed framework in urban water management and climate adaptation studies.

Overall, the results confirm that combining local terrain structure with global hydrological observations enhances urban water balance assessment and provides a more realistic representation of hydrological processes.

6. CONCLUSIONS

The integration of ALS-derived surface classification with hydrological datasets enables a more comprehensive understanding of urban water dynamics. The dominance of seasonal and stochastic variability over long-term trends suggests that local hydrological instability is primarily driven by short-term climatic variability and surface-structure characteristics rather than by monotonic climate change. The results of the analysis can be summarized in the following key findings:

1. ALS data enables precise classification of permeable and impervious surfaces.
2. The WB in the study area exhibits pronounced seasonal variability.
3. No statistically significant long-term monotonic trend was detected.
4. Drought severity is characterized by alternating wet and dry periods.
5. The integration of ALS and satellite-based hydrological data improves environmental assessment in urbanized areas.

Overall, the study developed and applied an integrated methodology linking high-resolution terrain-structure detection with large-scale hydrological observations to assess urban water-balance dynamics. By combining ALS-derived permeability classification with GLDAS and GRACE datasets, a consistent multi-scale analytical framework was established.

The automatic terrain classification revealed a predominance of permeable surfaces within the study area, which partially explains the relatively low surface runoff values and emphasizes the importance of spatial structure in shaping hydrological responses. Time-series analysis demonstrated that WB variability is primarily governed by seasonal and stochastic components rather than long-term trends.

The results show that integrating detailed ALS-based terrain information with satellite hydrological products significantly improves the interpretation of urban water-cycle dynamics. The proposed workflow provides a transferable methodological framework applicable to other urban environments, supporting sustainable water management and climate-adaptation strategies at local scales.

In addition, the presented framework demonstrates the potential of integrating high-resolution remote sensing data with global hydrological datasets for urban-scale environmental studies. Such a multi-source approach enables simultaneous consideration of local surface characteristics and large-scale climatic controls, which is essential for understanding complex urban hydrological responses. The methodology can therefore support more reliable water-resource assessments and provide valuable input for urban planning, stormwater management, and climate-adaptation strategies in rapidly changing urban environments.

REFERENCES

1. Wałęga, A, Radecki-Pawlik, A, Cupak, A, Hathaway, J and Pukowiec, M 2019. Influence of Changes of Catchment Permeability and Frequency of Rainfall on Critical Storm Duration in an Urbanized Catchment—A Case Study, Cracow, Poland. *Water* **11**, 2557.
2. Pasquier, U, Vahmani, P and Jones, AD 2022. Quantifying the City-Scale Impacts of Impervious Surfaces on Groundwater Recharge Potential: An Urban Application of WRF–Hydro. *Water* **14**, 3143.
3. Mazrooei, A, Reitz, M, Wang, D and Sankarasubramanian, A 2021. Urbanization Impacts on Evapotranspiration Across Various Spatio-Temporal Scales. *Earth’s Future* **9** (8).
4. Liu, K, Li, X and Wang, S 2021. Characterizing the spatiotemporal response of runoff to impervious surface dynamics across three highly urbanized cities in southern China from 2000 to 2017. *International Journal of Applied Earth Observation and Geoinformation* **100**, 102331.
5. Salazar, JF, Molina, RD, Zuluaga, JI and Gomez-Velez, JD 2024. Wetting and Drying Trends in the Land–Atmosphere Reservoir of Large Basins Around the World. *Hydrology and Earth System Sciences* **28**, 2919–2947.
6. Seager, R, Neelin, D, Simpson, I, Liu, H, Henderson, N, Shaw, T, Kushnir, Y, Ting, M and Cook, B 2014. Dynamical and Thermodynamical Causes of Large-Scale Changes in the Hydrological Cycle over North America in Response to Global Warming. *Journal of Climate* **27**, 7921-7948.
7. Zhu, J, Yin, D, Li, X, Zhu, R and Zheng, H 2024. Divergent Determinants on Interannual Variability of Terrestrial Water Cycle Across the Globe. *Science of the Total Environment* **945**, 174046.
8. Claessens, L, Hopkinson, C, Rastetter, E and Vallino, J 2006. Effect of historical changes in land use and climate on the water budget of an urbanizing watershed. *Water Resources Research* **42**.
9. Yilmaz, YA, Sen, OL and Turuncoglu, UU 2019. Modeling the Hydroclimatic Effects of Local Land Use and Land Cover Changes on the Water Budget in the Upper Euphrates–Tigris Basin. *Journal of Hydrology* **576**, 596–609.
10. Guizani, D, Buday-Bódi, E, Tamás, J and Nagy, A 2024. Enhancing water balance assessment in urban areas through high-resolution land cover mapping: Case study of Debrecen, Hungary. *Environmental Challenges* **15**,100906.
11. Dujardin, J, Batelaan, O, Canters, F, Boel, S, Anibas, C and Bronders, J 2011. Improving surface–subsurface water budgeting using high resolution satellite imagery applied on a brownfield. *Science of the Total Environment* **409**, 800-809.

12. Nigatu, ZM, Fan, D, You, W and Melesse, AM 2021. Hydroclimatic Extremes Evaluation Using GRACE/GRACE-FO and Multidecadal Climatic Variables over the Nile River Basin. *Remote Sensing* **13**, 651.
13. Sinha, D, Sayed, TH and Reager, J 2019. Utilizing combined deviation of precipitation and GRACE based terrestrial water storage as a metric for drought characterization: A case study over major Indian river basin. *Journal of Hydrology* **572**, 294-307.
14. Birylo, M, Rzepecka, Z and Nastula, J 2018. Assessment of the Water Budget from GLDAS Model. *Baltic Geodetic Congress (BGC-GEOMATICS 2018),* IEEE Xplore, 86-90.
15. Birylo, M, Blaszczak-Bak, W and Suchocki, C 2025. Application of GLDAS models and ALS point clouds in assessing the impact of modified evapotranspiration on the water budget. *Water Research* **283**, 123746.
16. Sun, AY, Save, H, Rateb, A, Jiang, P and Scanlon, BR 2024. Deciphering the Role of Total Water Storage Anomalies in Mediating Regional Flooding. *Geophysical Research Letters* **51**.
17. Rzepecka, Z, Birylo, M, Jerker, J, Cao, F and Pietroń, J 2024. Groundwater Storage Variations across Climate Zones from Southern Poland to Arctic Sweden: Comparing GRACE-GLDAS Models with Well Data. *Remote Sensing* **16**, 2104.
18. Hacker, C and Kusche, J 2024. How realistic are multi-decadal reconstructions of GRACE-like total water storage anomalies? *Journal of Hydrology* **645**, 132180.
19. Tapley, BD, Watkins, MM, Flechtner, F, Reigber, C, Bettadpur, S, Rodell, M, Sasgen, I, Famiglietti, JS, Landerer, FW, Chambers, DP, Reager, JT, Gardner, AS Save, H Ivins, ER Swenson, SC Boening, C, Dahle, C, Wiese, DN, Dobslaw, H, Tamisiea, ME and Velicogna, I 2019. Contributions of GRACE to understanding climate change. *Nature Climate Change* **9**, 358-369.
20. Richey, AS, Thomas, BF, Lo, M-H Reager, JT, Famiglietti, JS, Voss, K, Swenson, S and Rodell, M 2015. Quantifying renewable groundwater stress with GRACE. *Water Resources Research* **51**, 5217-5238.
21. Zhao, MAG, Velicogna, I and Kimball, JS 2017. A global gridded dataset of GRACE drought severity index for 2002–14: Comparison with PDSI and SPEI and a case study of the Australia Millennium drought. *Journal of Hydrometeorology* **18,** 2117-2129.
22. Swenson, SC and Lawrence, DM 2014. Assessing a dry surface layer-based soil resistance parameterization for the Community Land Model using GRACE and FLUXNET-MTE data. *Journal of Geophysical Research: Atmospheres* **119**, 10299-10312.
23. Wang, W, Cui, W, Wang, X and Chen, X 2016. Evaluation of GLDAS-1 and GLDAS-2 Forcing Data and Noah Model Simulations over China at the Monthly Scale. *Journal of Hydrometeorology* **17**, 935-953.
24. Rodell, M, Houser, PR, Jambor, U, Gottschalck, J, Mitchell, K, Meng, CJ, Arsenault, K, Cosgrove, B, Radakovich, J, Bosilovich, M, Entin, JK, Walker, JP, Lohmann, D and Toll, D 2004. The Global Land Data Assimilation System. *Bulletin of the American Meteorological Society* **85**, 381–394.
25. Penman, HL 1948. Natural evaporation from open water, bare soil and grass. *Proceedings of the Royal Society of London. Series A. Mathematical and Physical Sciences* **193**, 120–145.
26. Monteith, JL, Szeicz, G and Waggoner, PE 1965. The Measurement and Control of Stomatal Resistance in the Field. *Journal of Applied Ecology* **2**, 345.
27. Błaszczak-Bąk, W, Birylo, M, Biłozor, A, Cieślak, I and Janicka, J 2025. The Impact of Urbanization and Infrastructure Development on Local Flood Risk in Tomaszkowo: Hydrological Analysis and Spatial Planning. *Applied Sciences* **15**, 10863.
28. Brabec, E, Schulte, S and Richards, PL 2002. Impervious surfaces and water quality: a review of current literature and its implications for watershed planning. *Journal of Planning Literature* **16**, 499-514.